TRANSIENT SIMULATION OF THE RL-10A-3-3A ROCKET ENGINE

Francesco Di Matteo[†], Marco De Rosa[‡*], Marcello Onofri[†]
[†]Sapienza University of Rome
Dipartimento di Ingegneria Meccanica e Aerospaziale, Via Eudossiana 18, I-00184 Rome, Italy
[‡]ESA-ESTEC, Propulsion Engineering
Keplerlaan 1, 2201AZ Noordwijk, Netherlands

Abstract

Modelling on transient phase operations of a liquid rocket engine is a challenging task because most of the engine components are required to work at extreme operating conditions; start-up and shut-down operations feature very complex phenomena such as combustion instabilities, reverse flow in the pumps, turbopumps operating far from design conditions and two-phase flows that cannot be neglected when design studies of an engine are to be performed or the assessment of the valve opening sequence has to be done.

For these reasons simulations of the ignition transient phase and the shut-down phase become necessary in order to reduce the experimental tests and increase the engine safety and reliability. The RL-10 engine (model RL-10A-3-3A) has been chosen for several reasons, among which the good availability of engine construction data, performance and tests results in open literature. The start-up transient phase of the Pratt&Whitney RL-10 engine has been taken as validation case. The results of the start-up simulation will be summarised in the paper.

In this study the shut-down operation of the RL-10A-3-3A liquid rocket engine is modelled, analysed and simulated by means of a system simulation tool, EcosimPro, an object oriented tool capable of modelling various kinds of dynamic systems and ESPSS, the European propulsion system library compatible with the platform.

A system approach is necessary to take into account all the interactions between all the components of an engine. This choice is fundamental if a detailed estimation of the engine transient behaviour is the task. The layout simulated by the code encompasses the complete feeding system from the tanks down to the turbopump subsystems, the valves, the pipes, the thrust chamber's inlets, the heat transfer in the regenerative circuit and the chemical reactions inside the combustion chamber.

The main subsystem models of this engine will be described and their validation will be presented alongside the description of the integrated model of the entire engine. The results of the shut-down simulation will be then compared with experimental data.

Nomenclature

C_o	Turbine exit sound velocity, m/s
H	Flow total enthalpy, kJ/kg
h	Dimensionless pump head, -
h_c	Convective heat transfer coefficient, W/m^2·K
n	Rotational speed ratio, -
N	Turbine velocity ratio, -
$\dot{m}$	Mass flow rate, kg/s
Q	Volumetric mass flow rate, m^3/s
Q^+	Turbine mass flow coefficient, -
$\dot{q}$	Heat flux, W/m^2
r	Turbine blade mean radius, m
ST	Turbine specific torque, -
St	Stanton number, -
T	Temperature, K
TDH	Pump total dynamic head, m
β	Dimensionless pump torque, -
θ	Dimensionless pump variable, -
λ	Thermal conductivity, W/m·K
ν	Volumetric flow rate ratio, -
ξ	Friction coefficient, -
Π	Turbine total to total pressure ratio, -
ρ	Density, kg/m^3
σ	Radiative heat transfer coefficient, W/m^2·K^4
τ	Mechanical torque, N·m
ω	Rotational speed, rad/s

Subscript

aw	adiabatic wall
R	rated condition
ref	reference condition
th	throat condition
w	wall

*Corresponding author: francesco.di.matteo@esa.int

1 Introduction

This paper describes the development and the validation of a computational transient model of the RL-10A-3-3A rocket engine. The RL-10 engine is based on an expander cycle, in which the fuel is used to cool the main combustion chamber and the thermal energy added to the fuel drives the turbopumps. The RL-10A-3-3A developed by Pratt & Whitney under contract to NASA, presents a long historical heritage and incorporates component improvements with respect to the initial RL-10A-1 engine.

The RL-10 engine has been used extensively as object of simulations in the past years [1, 2, 3, 10, 9]. The work pre-

sented in this paper aims to show the improvements made in terms of modelling with respect to the previously cited works; indeed, the model present here features a 1-D discretisation not only in the cooling jacket model, but also for most of the other components, such as the combustion chamber, the venturi duct and the other pipes.

In previous works [3], large use of look-up-tables has been made to describe the components behaviour such as the Venturi pipe or the cooling channels; the combustion chamber has been modelled as a built-in set of hydrogen/oxygen combustion tables as well. Here, a fully 1-D discretised chamber and nozzle features a chemical equilibrium model based on Gibbs energy minimization for each section along the chamber. The present model also contains an injector plate model representative not only of the capacitive effect of the injector dome mass but also of the convective and radiative heat fluxes from the chamber to the injector and of the conductive heat flux between the fuel and oxidiser injector domes. The thermal model used for the cooling jacket component is modelled as a "real" one and a half counterflow cooling jacket.

2 RL-10 architecture

The RL10A-3-3A includes seven engine valves as shown in Figure 1. The propellant flows to the engine can be shut off using the Fuel Inlet Valve (FINV) and the Oxidizer Inlet Valve (OINV). The fuel flow into the combustion chamber can be stopped by the Fuel Shut-off Valve (FSOV) located just upstream of the injector plenum. The valve serves to prevent fuel flow into the combustion chamber during the cool-down period and provide a rapid cut-off of fuel flow during engine shut-down [12].

The fuel interstage and discharge cool-down valves (FCV-1 and FCV-2) are pressure-operated, normally open sleeve valves. The functions of these valves are the following [12]:

- allow overboard venting of the coolant for fuel pump cool-down during engine pre-chill and pre-start
- provide first stage fuel pump bleed control during the engine start transient (for the FCV-1)
- provide fuel system pressure relief during engine shut-down

The Thrust Control Valve (TCV) is a normally closed, closed-loop, variable position bypass valve used to set engine thrust by regulation of turbine power. TCV is also used to control thrust overshoot at start and maintain constant chamber pressure during steady-state operation. As combustion chamber pressure deviates from the desired value, action of the control allows the turbine bypass valve to vary the fuel flow through the turbine [12].

The Oxidizer Control Valve (OCV) is used to set the engine mixture ratio. OCV has two orifices: one regulates the main oxidizer flow (OCV-1) and the other controls the bleed flow required during engine start (OCV-2). The main-flow orifice in the OCV is actuated by the differential pressure across the LOX pump. The OCV valve is a normally closed, variable position valve.

The Venturi upstream of the turbine is designed to help stabilize the thrust control.

Ducts and manifolds in the RL10 are generally made out of stainless-steel and are not insulated.

Name	Value	Units
Fuel Turbopump		
1st stage impeller diameter	179.6	[mm]
1st stage exit blade height	5.8	[mm]
2nd stage impeller diameter	179.6	[mm]
2nd stage exit blade height	5.588	[mm]
Oxidiser Turbopump		
Impeller diameter	106.7	[mm]
Exit blade height	6.376	[mm]
Turbine		
Mean line diameter	149.86	[mm]
Ducts & Valves		
FINV flow Area	0.0041	[m^2]
FCV-1 flow Area	0.00038	[m^2]
FCV-2 flow Area	0.00019	[m^2]
Venturi (inlet - throat)	0.0023 - 0.00067	[m^2]
TCV flow Area [a]	$1.01E^{-5}$ [b]	[m^2]
FSOV flow Area	0.0021	[m^2]
OINV flow Area	0.0031	[m^2]
OCV flow Area [a]	$3.96{\cdot}10^{-4}$ [b]	[m^2]
Cooling jacket		
Number of tubes	180	[-]
Channel width at throat	2.286	[mm]
Channel height at throat	3.556	[mm]
Typical hot wall thickness	0.3302	[mm]
Thrust chamber		
Chamber diameter	0.1303	[m]
Throat diameter	0.0627	[m]
Nozzle area ratio	61	[-]
Chamber/nozzle length	1.476	[m]

Table 1: RL-10A-3-3A construction data [3]

[a] values at nominal full-thrust condition
[b] flow area includes the discharge coefficient

2.1 Description of the start-up sequences

The RL-10 engine starts by using the pressure difference between the fuel tank and the nozzle exit (upper atmospheric pressure), and the ambient heat stored in the metal of the cooling jacket walls. The engine "bootstraps" to full-thrust within two seconds after ignition.

A typical plot of the valve movement during engine start is shown in Figure 2. To initiate start, the FSOV is opened and the fuel-pump discharge cool-down valve (FCV-2) is closed. The interstage cool-down valve (FCV-1) remains partially open in order to avoid stalling of the fuel pump during engine acceleration. The pressure drop between the fuel inlet and the combustion chamber drives fuel through the cooling jacket,

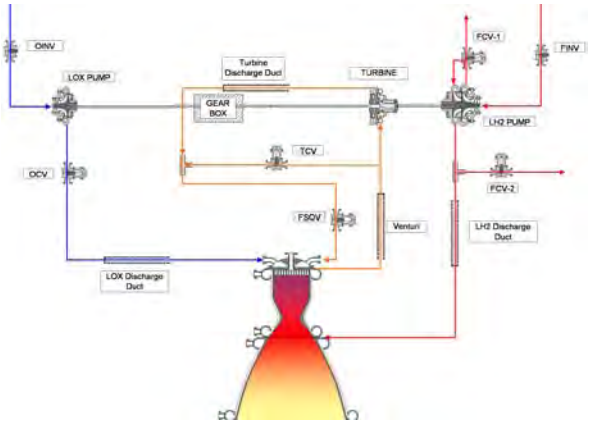

Figure 1: RL-10A-3-3A engine diagram

picking up heat from the warm metal. This pressure difference also drives the heated fluid through the turbine, starting rotation of the pumps, which drive more propellant into the system. At start, the OCV also closes partially, restricting the flow of oxygen into the combustion chamber. This is done to limit chamber pressure and ensure a forward pressure difference across the fuel turbine after ignition of the thrust chamber.

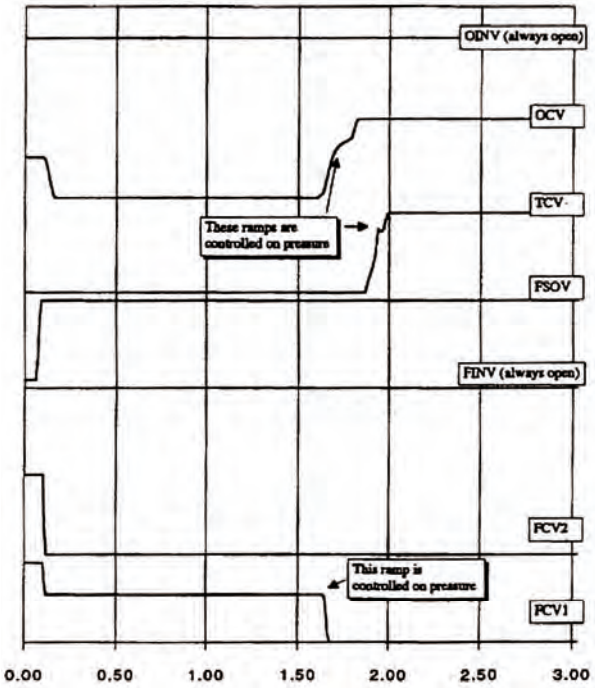

Figure 2: RL-10A-3-3A Valve schedule for Start-up Simulation [3]

Ignition of the main combustion chamber usually occurs approximately 0.3 seconds after the main-engine start signal (t = 0) is given (for first-burns). The ignition source is a torch igniter powered by an electric spark. The ignited combustion chamber provides more thermal energy to drive the turbine.

As the turbopumps accelerate, engine pneumatic pressure is used to close the interstage cool-down valve completely and open the OCV at pre-set fuel and LOX pump discharge pressures. The OCV typically opens very quickly and the resultant flood of oxygen into the combustion chamber causes a sharp increase in system pressures. During this period of fast pressure rise, the thrust control valve (TCV) is opened, regulated by a pneumatic lead-lag circuit to control thrust overshoot. The engine then settles to its normal steady-state operating point.

2.2 Description of the shut-down sequence

The RL-10 engine switches off at the end of its mission, after the steady state phase. The Fuel Shut-off Valve (FSOV) and the Fuel Inlet Valve (FINV) close as the FCV-1 and FCV-2 valves open, allowing fuel to drain out of the system through the overboard vents. The combustion process is soon starved of fuel and the flame extinguishes. The Oxidiser Control Valve (OCV) and the Oxidiser Inlet valve (OINV) begin to close next, cutting off the flow of oxygen through the engine. The turbopump decelerates due to friction losses and drag torque created by the pumps as they evacuate the remaining propellants from the system. A typical plot of the valve movement during engine shut-down is shown in Figure 3.

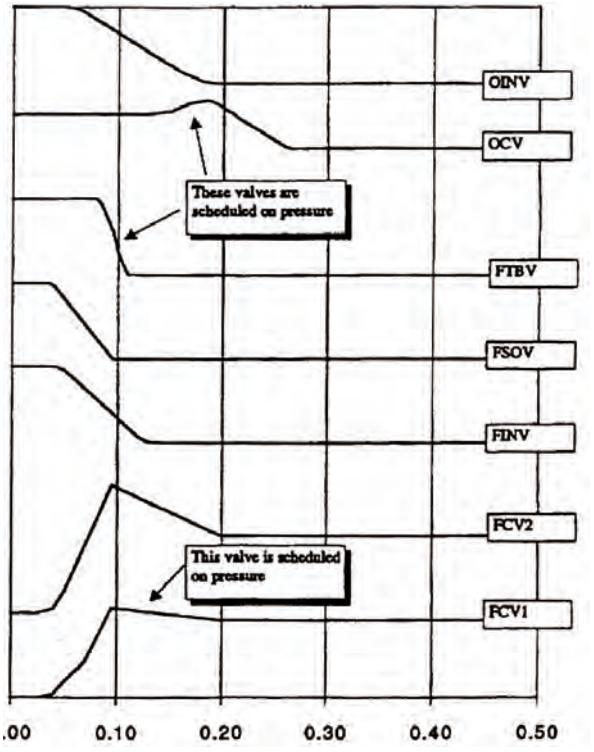

Figure 3: RL-10A-3-3A Valve schedule for Shut-down Simulation [3]

During the engine shut-down, a different combination of off-design conditions appears to exist, including pump cavitation and reverse flow. Proper simulation of these effects is

complicated by their interaction with each other. From available test data and simulation output, it appears that as the fuel inlet valve closes and the cool-down valves open, the pump first cavitates due to a combination of changes in pump loading and cut-off of the inlet flow. The cavitation causes the pump performance to degrade rapidly until the pump cannot prevent the reverse flow of fluid as it comes backward through the cooling jacket. When the reversed flow reaches the closed fuel inlet valve, however, extreme transients of pressure and flow are created. Similar effects are encountered in the LOX pump during shut-down as well.

The pump head and torque performance characteristics during, this period of operation are, of course, not extensively documented in test data. The generic pump characteristics found in References [13] and [4] have been used to extend the performance maps for cavitation and reverse flow.

The pump map extensions for engine shut-down are included in Figures 4 and 5, page 5. Although the engine start-up and shut-down models use the same pump performance maps (which should be able to cover all the pump regimes), the cavitation and reverse flow effects also require additional modelling effort, that has not been implemented into this model yet.

3 Modelling

The development of the RL-10 engine transient model was conducted with a commercial tool called EcosimPro and the European Space Propulsion System Simulation library (ESPSS) which enables the modelling and analysis of propulsion systems for both spacecraft and launcher applications. The ESPSS is a set of libraries written to model all aspects of a propulsion system.

3.1 Fluid Properties

In a cryogenic rocket engine, the variations of fluid properties during the transient phase have a huge impact on the engine performances and behaviour, most notably on the coolant side: mass flow rate, pressure losses, heat transfers inside the cooling jacket, etc. The fluid properties library is in charge of the calculation of fluid properties. Functions available on this library are mainly used by the 1-D fluid flow library for the simulation of fluid systems. Real fluids properties are considered in the model for the couple LH_2 and LO_2, by tables depending on both pressure and temperature derived from NIST database [11]. This class covers liquid, superheated, supercritical and two-phase fluids. Two-phase, two fluids mixtures of a real fluid in any thermodynamic state with a non-condensable gas (ideal) are allowed, as in the case of pre-start phase where propellants are in contact with gaseous helium. The homogeneous equilibrium model is used to calculate the properties (quality, void fraction, etc..) of a real fluid in two-phase conditions, with or without a non-condensable gas mixture.

3.2 Turbomachinery modelling

Pumps

The pump model makes use of performance maps for head and resistive torque. The pump curves are introduced by means of fixed 1-D data tables defined as functions of a dimensionless variable θ that preserves homologous relationships in all zones of operation. θ parameter is defined as follows:

$$\theta = \pi + \arctan(\nu/n) \tag{1}$$

where ν and n are the reduced flow and the reduced speed respectively:

$$\nu = \frac{Q}{Q_R} = \frac{\dot{m}_{in}/\rho_{in}}{Q_R} \qquad\qquad n = \frac{30\,\omega\,/\pi}{rpm_R} \tag{2}$$

The dimensionless characteristics (head and torque) are defined as follows:

$$h = \frac{TDH\ /\ TDH_R}{n^2+\nu^2} \qquad\qquad \beta = \frac{\tau\ /\ \tau_R}{n^2+\nu^2} \tag{3}$$

this method eliminates most concerns of zero quantities producing singularities. To simplify the comparison with generic map curves, these relations are normalized using the head, torque, speed and volumetric flow at the point of maximum pump efficiency. These maps have been created as a combination of available test data provided by Pratt&Whitney [3] and generic pump performance curves [4] (see Figures 4 and 5, test data range in grey). Additional maps were established (not shown here), giving a corrective factor on the pump torque, function of the rotational speed ratio (also provided by P&W). The enthalpy flow rise is a function of the absorbed power while the evaluation of the mass flow rate is performed through an ODE.

$$\begin{cases} (\dot{m}\,h)_{out} = \tau\cdot\omega - (\dot{m}\,h)_{in} \\ I\dfrac{d\dot{m}}{dt} = \left(P+\dfrac{1}{2}\rho v^2\right)_{out} - \left(P+\dfrac{1}{2}\rho v^2\right)_{in} - g\rho_{in}TDH \end{cases}$$

Because of the presence of the FCV-2 valve between the first and the second stage, the fuel pump has been modelled with two separated pump components, one for each stage. Since the oxidiser pump has only one stage, it has been modelled with one component instead. For each pump model the main nominal parameters have been calculated by a numerical code specifically developed to find the nominal value of the outlet pressure, the pump torque τ_p, the total dynamic head TDH, the pump efficiency η_p and the specific speed Ns by use of the pump head and pump efficiency curves provided by Pratt & Whitney [3]. Since no official values of the propellants leak to the gear box were found, an iterative procedure was adopted to find the correct value of the mass flow rate and the outlet pressure in each stage.

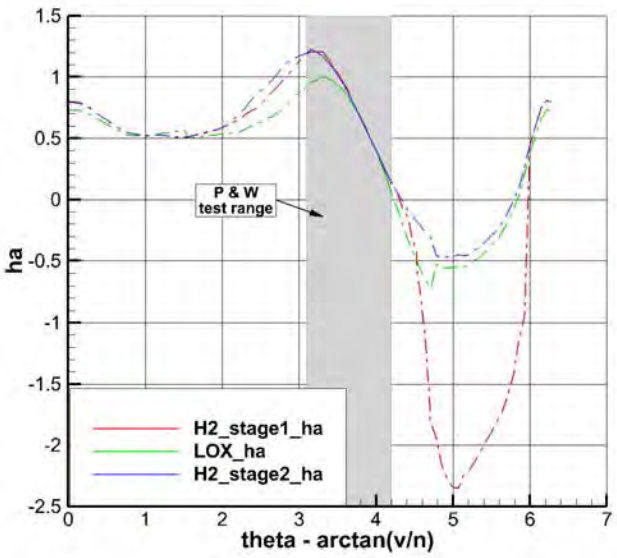

Figure 4: Extended Head map for LOX and Fuel pumps

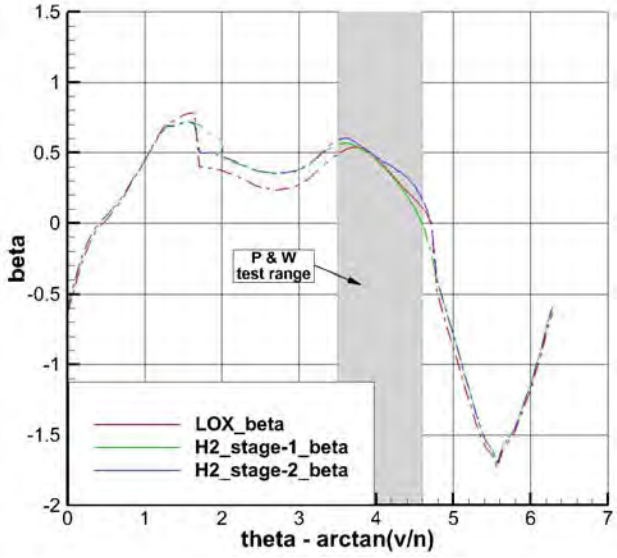

Figure 5: Extended Torque map for LOX and Fuel pumps

Turbine

The turbine performance maps provided by Pratt&Whitney depict the combined performance of the two stages (see Figures 6 and 7). The first figure describes the effective area (area times discharge coefficient) as a function of velocity ratio (U/C_o) for several different pressure ratios. The second one describes the combined two-stage turbine efficiency as a function of velocity ratio (U/C_o) as well.

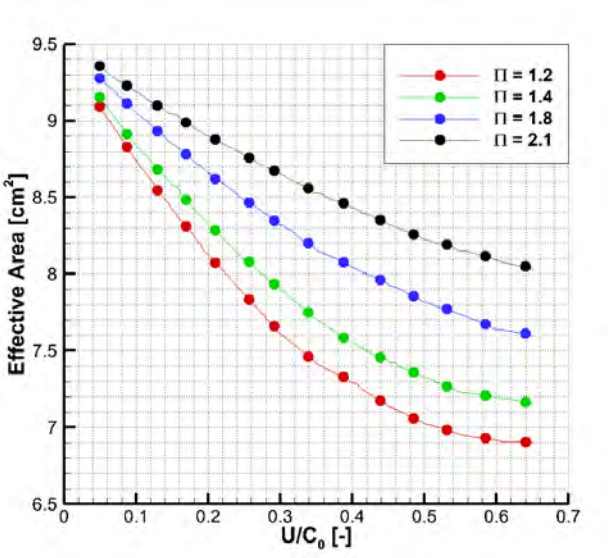

Figure 6: Effective Area map for the Turbine from P&W [3]

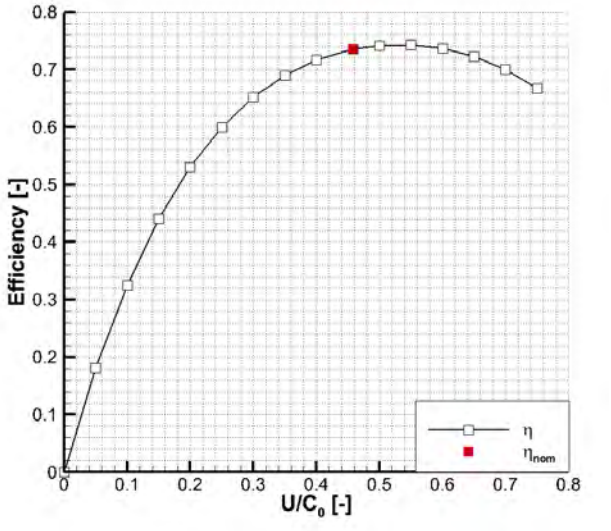

Figure 7: Efficiency map for the Turbine from P&W [3]

In the present study, Pratt & Whitney performance maps are transformed to obtain the turbine performance maps used in the ESPSS turbine model. These maps (mass flow coefficient and specific torque) are introduced by means of 2-D

input data tables as a function of velocity ratio and pressure ratio:

$$N = \frac{r \cdot \omega}{C_o} \qquad \Pi = P_{01} \,/\, P_{02} \tag{4}$$

and the mass flow coefficient and specific torque are defined as:

$$Q^+ = \frac{\dot{m}_{map} \cdot C_o}{r^2 \, P_{01}} \qquad ST = \frac{\tau}{r \, \dot{m}_{map} \, C_o} \tag{5}$$

According to Eq. 5 and to the power balance equation $\tau \cdot \omega = \dot{m} \, \eta \, \Delta h_{is}$ we obtain the non-dimensional parameters as function of velocity ratio and pressure ratio using data from the P&W maps:

$$\tau \cdot \omega = \dot{m} \, \eta(\Pi) \, \Delta h_{is} \quad \Rightarrow \quad ST \, r \, \dot{m} \, C_o \cdot \omega = \dot{m} \, \eta(\Pi) \, \Delta h_{is}$$
$$\Rightarrow \quad ST \, C_o^2 \, N = \eta(\Pi) \, \Delta h_{is} \quad \Rightarrow$$
$$ST(\Pi, \, N) = \frac{\eta(\Pi) \, \Delta h_{is}}{C_o^2 \, N}$$

and for the Q^+ parameter we just need to calculate the turbine mass flow as function of N and Π:

$$A_{eff} = C_D \cdot A = f(\Pi, \, N)$$
$$\dot{m} = C_D \cdot A \cdot \sqrt{P_{01} \, \rho_{01} \, \frac{2\gamma}{\gamma - 1} \left[\Pi^{-\frac{2}{\gamma}} - \Pi^{-\frac{\gamma+1}{\gamma}} \right]}$$

This formulation is based on the assumption that no chocking conditions occur during the transient and at steady conditions of the turbine component, plausible because subsonic.

3.3 Thrust chamber and cooling jacket modelling

The thrust chamber component, inherited from the original ESPSS library [7], represents a non adiabatic 1-D combustion process inside a chamber for liquid or gas propellants. The equilibrium combustion gases properties (molar fraction, thermodynamic and transport properties) are calculated for each chamber volume (node) using the minimum Gibbs energy method [8] as a function of the propellant's mixture molar fractions, inlet conditions and chamber pressure. Transient chamber conditions (pressures, temperatures, mass flows and heat exchanged with the walls) are derived from 1-D transient conservation equations. A mixture equation between the injected propellants and the combustion gases is applied. From the definition of the mixture ratio MR and derivation, the following dynamic equation gives the MR evolution:

$$\dot{m}_{ox} = MR \, \dot{m}_{fu} + \frac{d}{dt} \, (MR) \, \frac{\rho V_c}{1 + MR} \tag{6}$$

Combustion takes place when mixture ratio is within the allowed limits, the ignition flag is active and a minimum time (ignition delay) τ has elapsed. Mass, energy and momentum equations are basically the same as in the pipe component with variable cross area, Equations (7), (8).

$$\frac{\partial \boldsymbol{u}}{\partial t} + \frac{\partial f(\boldsymbol{u})}{\partial x} = S(\boldsymbol{u}) \tag{7}$$

where

$$\boldsymbol{u} = A \begin{bmatrix} \rho \\ \rho x^{nc} \\ \rho v \\ \rho E \end{bmatrix}; \quad f(\boldsymbol{u}) = A \begin{bmatrix} \rho v \\ \rho v x^{nc} \\ \rho v^2 + P \\ \rho v H \end{bmatrix};$$
$$S(\boldsymbol{u}) = \begin{bmatrix} 0 \\ 0 \\ -0.5(d\xi/dx)\rho \, v|v|A + \rho g A + P(dA/dx) \\ \dot{q}_w(dA_{wet}/dx) + \rho g v A \end{bmatrix} \tag{8}$$

The centred scheme is used to discretise the chamber, using a staggered mesh approach (see Figure 8). The chamber contour has been divided in 40 volumes: 10 in the subsonic section, 10 from the throat to cooling jacket inlet manifold and the last 20 volumes from there until the nozzle exit. The mesh has been stretched and compressed in order to capture the main fluid-dynamic phenomena occurring along the chamber (fluid acceleration, heat flux in the throat region, Mach evolution). The RL10A-3-3A has a silver throat insert that creates

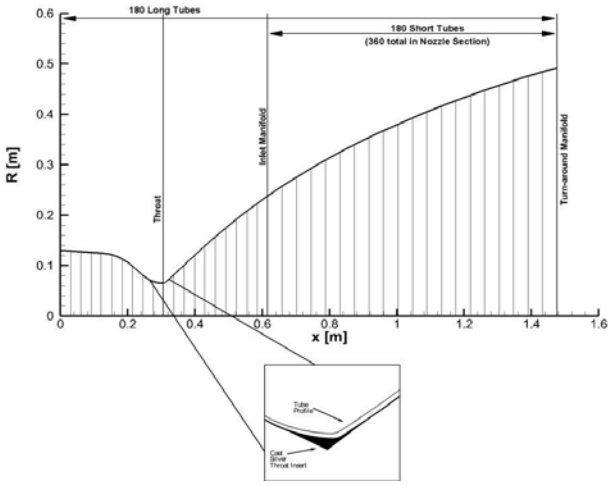

Figure 8: RL-10A-3-3A chamber contour [3] and discretisation

a sharp edge, not typically used and difficult for EcosimPro to model. For this reason a scale coefficient factor named R_{ins} has been added into the code; the coefficient is function of the silver insert geometry and the effective throat area considering the reduction due to viscous effects.

The walls represented by thermal components in the *Cooling Jacket* component are not included in the chamber model, but are taken as a boundary for the heat exchange calculation instead:

$$\dot{q}_w = h_c A_{wet}(T_{aw} - T_w) + \sigma A_{wet}(T_{core}^4 - T_w^4) \tag{9}$$

In the combustion chamber component the heat transfer coefficient h_c can be evaluated by different correlations (original Bartz equation, modified Bartz equation, Pavli equation). Refer to paper [5] for a detailed description of the heat transfer correlation models. An heat transfer simulation campaign at subsystem level has been performed in order to compare the different correlations and choose the most suitable. Then the modified Bartz equation has been chosen. The Bartz equation has been rewritten in a Stanton type form and modified with correction factors calculated according to chamber geometry:

$$St_{Bartz}=0.026\left(\frac{\mu_{ref}^{0.2}}{c_{p,ref}^{0.6}}\right)\left(\frac{\lambda_{ref}}{\mu_{ref}}\right)^{0.6}(\dot{m})^{-0.2}A^{0.1}\left(\frac{\pi D_{th}/4}{R_{curv}}\right)^{0.1}K_T\,K_x \tag{10}$$

The RL10A-3-3A injector plate is rather complicated, involving several different injector element designs. Most of the injector elements are co-axial, the hydrogen in injected through annular orifices around each LOX element. The outer concentric row of elements, however, inject hydrogen only (which will affect wall cooling). It is possible that some of the differences encountered in the heat transfer model are due to not including this film cooling effect in those predictions.

The injector plate composed by injectors and injector domes is modelled by a component that takes into account the convective and radiative heat transfer between the fluid in the first volume of the chamber and the face plate, and evaluates the conductive and capacitive effect of the injector walls in an accurate way, representative of a generic injector head [5]. In order to reflect the thermal capacity of the injector plate, the actual mass and the material properties of the dome have been used into the model (see Table 1). For the oxidiser and fuel injector orifices, *junctions* components have been specifically modelled to match the mass flow and the pressure drop. Nevertheless, the geometrical construction data of the injector orifices have not been modified but used to assess the pressure drop coefficient ζ; for each propellant injectors, considering the orifice area as the sum of the overall injectors, it yields:

$$\left(\frac{P_{cc}}{\rho}+\frac{1}{2}v^2\right)-\left(\frac{P_{cav}}{\rho}\right)=-\frac{1}{2}\zeta v^2 \;\Rightarrow\; \Delta P=(1+\zeta)\frac{\dot{m}^2}{2\rho A^2}$$

The cooling jacket model is constructed of 360 stainless steel tubes of type 347SS properties. There are 180 short tubes, from inlet manifold to the turn-around one, and other 180 long tubes, from the turn-around manifold to the injector plate. The short and long tubes are arranged side-by-side in the nozzle section.

A new model structure has been developed and implemented just for the RL-10 cooling jacket subsystem. The model has been built with two *Tube* components, the first one simulating the short channels and the second describing the long channels. The two tubes are connected together thanks to a *Junction* component that models in this way the pressure drop caused by the turn-around manifold. The component developed is able to reproduce the peculiar pattern of the cooling channels in the nozzle section, where the long tubes are interspersed with the short tubes. The heat coming from the chamber is then distributed to both channels.

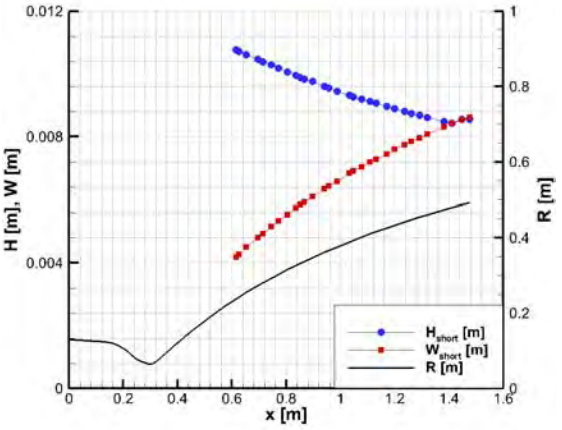

(a) Short channels width and height profile [14]

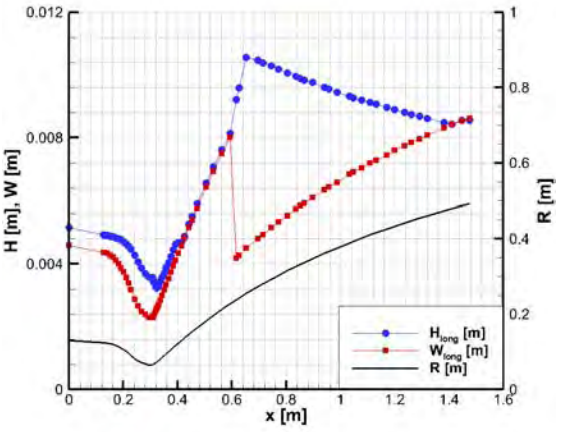

(b) Long channels width and height profile [14]

Figure 9: Cooling jacket channels profiles

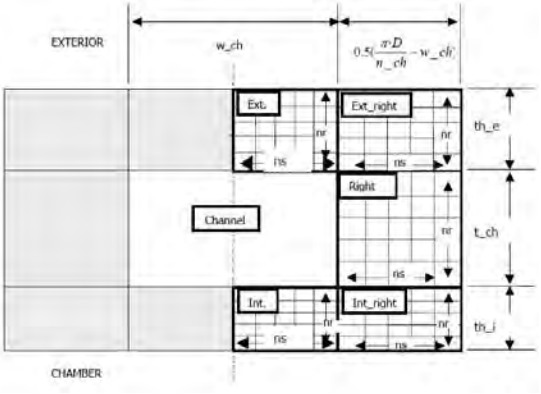

Figure 10: Cooling jacket wall mesh

The cooling jacket model is divided into a variable number of sections in axial direction. Every section is made of one fluid node of the *Tube* component (from FLUID_FLOW_1D library, see Equations (7),(8)), which is simulating the cooling channels and five slices of the "3D wall" components, which are simulating the metallic walls. The walls are divided in 5 different 3-D components as shown in Figure 9 (c); the contours of the actual height and width of the RL-10 channels are shown in Figure 9 (a, b). Each component has a 3-dimensional discretisation in tangential, radial and longitudinal direction (dx, dy, dz), respectively.

Since the cooling channel shape is not rectangular but slightly rounded, a detailed geometrical reconstruction has been performed to assess the effective exposed surface area, to maintain the original pressure drop and the coolant velocity evolution. To this purpose the Pratt&Whitney specification has been accepted regarding the angle of exposure which is around 112° [3].

3.4 Lines, valves and manifolds modelling

In addition to the various subsystem listed above, there are on the RL-10 engine a large number of lines valves and manifolds. Valves are modelled as zero dimensional components while the lines present in the engine are modelled via an area-varying non-uniform mesh 1-D scheme. Where possible and data were available a detailed geometrical reconstruction has been performed, as for the case of the Venturi pipe and the discharge turbine pipe.

4 Summary of the RL-10 engine start-up

The start-up transient phase has been taken as validation case and has been already described in a previous work [6]. Here a summary of the main results are shown for completion and clarity of the simulation procedure.

The results of start-up transient simulations ("Simulation" on the plots) were compared with measured data of a single ground test first-burn (P2093 Run 3.02 - Test 463, "Ground Test [3]" on the plots) [3] and with the simulation results of a previous work ("xx_sym [3]" on the plots) performed by a NASA team [3]. Since no detailed initial conditions along the engine were available, a simulation of the pre-start phase was necessary to obtain reasonable initial conditions for the engine start.

Figure 11 (a) shows the comparison between measured and predicted chamber pressure. The model matches the measured time-to-accelerate to within approximately 92 milliseconds (the "time-to-accelerate" is defined here as the time from 0 seconds at which the chamber pressure reaches 13.79 bar (200 psia)). The very first pressure rise at ≈0.3s represents the chamber ignition as mentioned above. The chamber pressure shows a "plateau" until the OCV opens. After the OCV opening, the chamber pressure rises very quickly and then stabilizes to the steady state condition thanks to the TCV valve closed loop control.

In Figure 11 (b) the LOX pump rotational speed is shown: the simulation result is in good agreement with experimental result. The difference in the rate of change of the pump speed between the simulation and experiment may be due to the uncertainty in the pump inertia distribution.

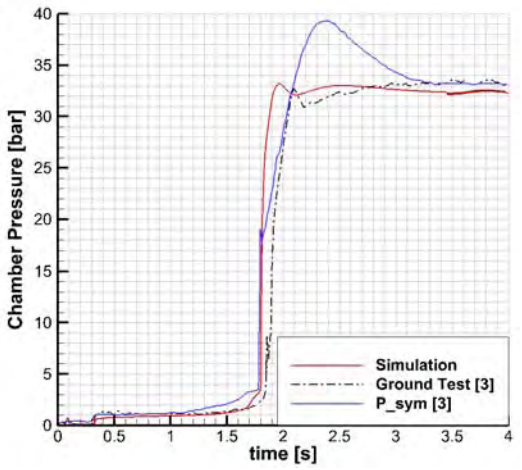

(a) Chamber Pressure

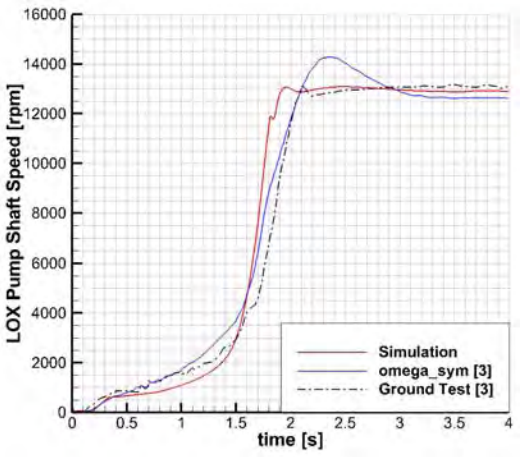

(b) LOX Pump Shaft Speed

Figure 11: Start-up transient results

5 RL-10 engine shut-down

The results of shut-down simulations ("Simulation" on the plots) were compared with measured data of a single ground test (P2093 Run 8.01 - Test 468, "Ground Test [3]" on the plots) [3] and with the simulation results of a previous work ("xx_sym [3]" on the plots) performed by the NASA team [3]. Due to the uncertainty related to the valves closing schedule made necessary to slightly trim the valve sequence (few ms). The original schedule and the valves positions profile has

been used as guideline. The modified shut-down sequence is illustrated in Figure 12.

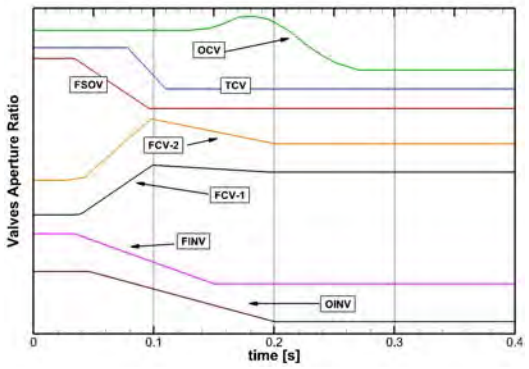

Figure 12: Valves closing sequence adopted in the simulation

Figure 13 (a) illustrates the combustion chamber pressure trend. Once the FSOV starts to close the chamber pressure decreases and this happens in both the simulations and the experimental data, showing a good agreement between them.

Figure 13 (b) shows predicted and measured pump speed for the Oxidiser propellant side. The discrepancies from the two models and the ground test measured data are imputable to uncertainties on the inlet conditions and initial operating point as well as on a precise distribution of the turbopump assemblies inertia.

Figures 14 (a, b) depict the LOX pump inlet and outlet pressures evolution. Regarding the pressure at the outlet of the pump, no special features are evident. Once the FSOV valve starts to close, the outlet pump pressure decreases because of the minor power delivered by the turbine.

Figure 14 (b) illustrates the inlet pressure instead. From the measured data we see an initial pressure decrease due to the pump conditions and then a recovery in the pressure to the complete closure of the OINV valve. This behaviour is barely reproduced by the simulation because of the lack of a cavitation model in the pump, hence the final pressure decrease is not as evident as in the experiment.

The engine propellant mass flows are depicted in Figures 14 (c) and 15 (a), for the oxidiser and the fuel respectively. The oxygen mass flow behaviour (Figure 14 (c)) is mainly function of the pump behaviour; it is interesting to underline that from analyses performed varying the opening/closing time of the valves, the role of the FCV valves becomes much more evident. The opening of the FCV valves decreases the turbine power, hence decreasing the propellant mass flow rate in the system in order to avoid mass flow rate surges of oxygen at the FSOV closure. In the end, the complete shut-off of the OINV valve extinguishes the propellant flow rate.

A more complex profile is present in the fuel flow plot as shown in Figure 15 (a): at the beginning of the shut-down phase the hydrogen mass flow at the engine inlet increases because of the opening of the FCV valves. Then the closure of the FSOV and of the FINV valve determine the mass flow shut-off. The simulation reproduces correctly what happens at inlet of the engine, even though the amount of mass flow venting through the FCV valves results too high determining a higher peak at the inlet respect to the one observed in the ground test. Another interesting point to be mentioned is that differently from the NASA results the "Simulation" line does not show any reverse flow at the inlet, coherently with the experimental data.

In Figure 15 (b), the measured data show a characteristic dip, rise and then falloff in the fuel venturi upstream pressure. This features is caused by the dynamic interaction of the fuel pump cool-down valve opening and main fuel shut-off valve closing. It is very likely that the absence of this peculiar behaviour inside our model is due to a not perfectly precise synchronization of the fuel valves closing schedules.

In Figure 15 (c), the jump in pump inlet pressure is due, in part, to reverse flow through the fuel pump. As already mentioned, a cavitation model for pump performance deterioration is not implemented so the pressure peak does not rise in the simulation result.

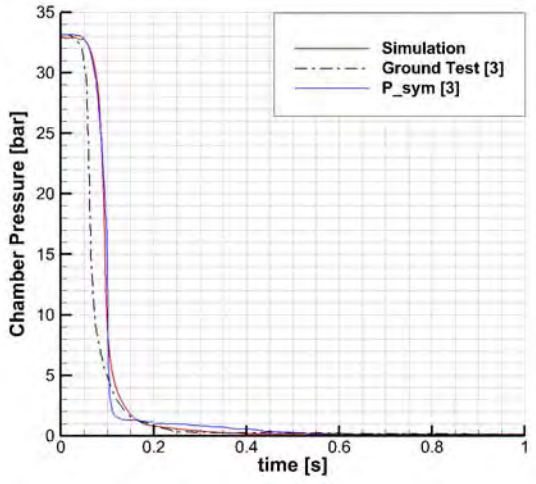

(a) Chamber Pressure

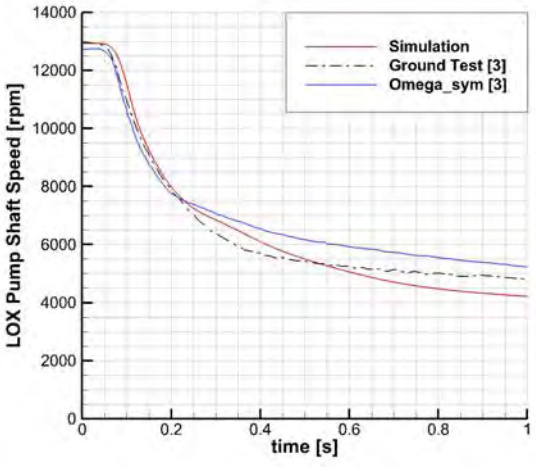

(b) LOX Pump Shaft Speed

Figure 13: Shut-down results - part 1

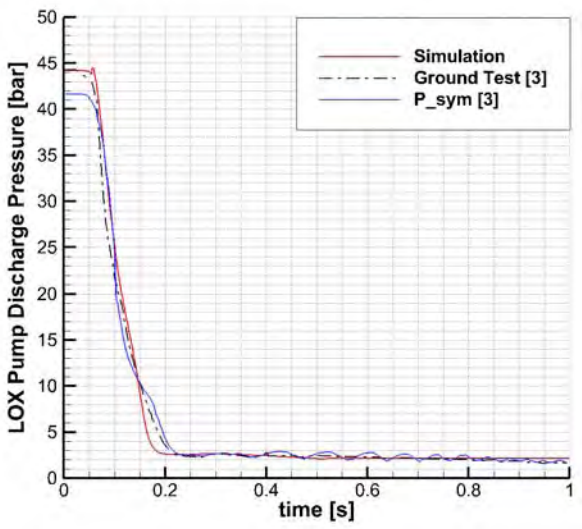

(a) LOX Pump Discharge Pressure

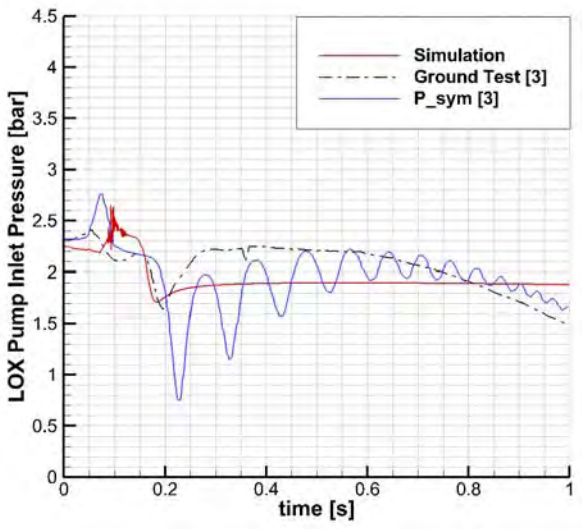

(b) LOX Pump Inlet Pressure

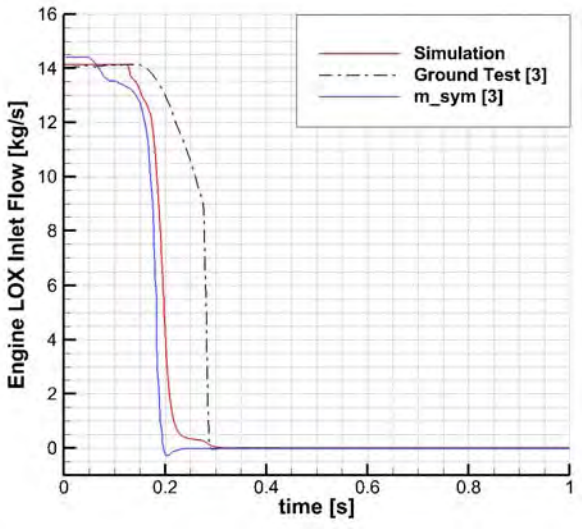

(c) LOX Engine inlet mass flow

Figure 14: Shut-down results - part 2

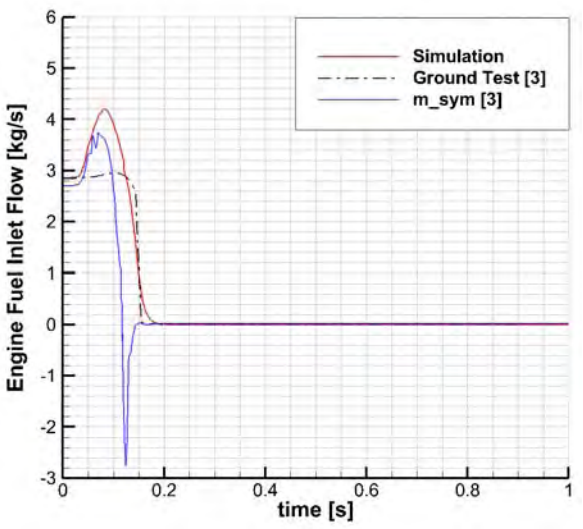

(a) Fuel Engine inlet mass flow

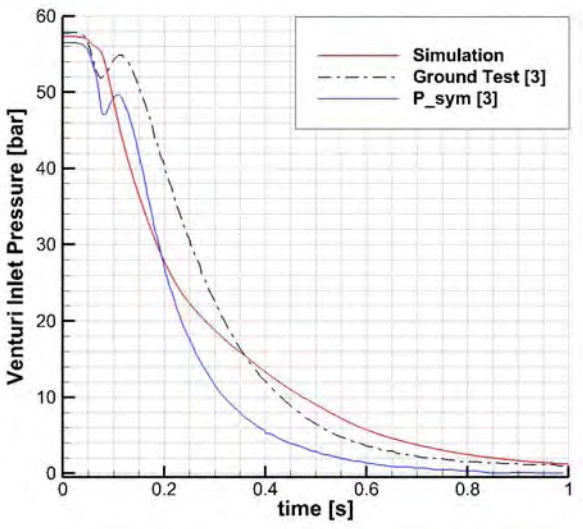

(b) Venturi inlet Pressure

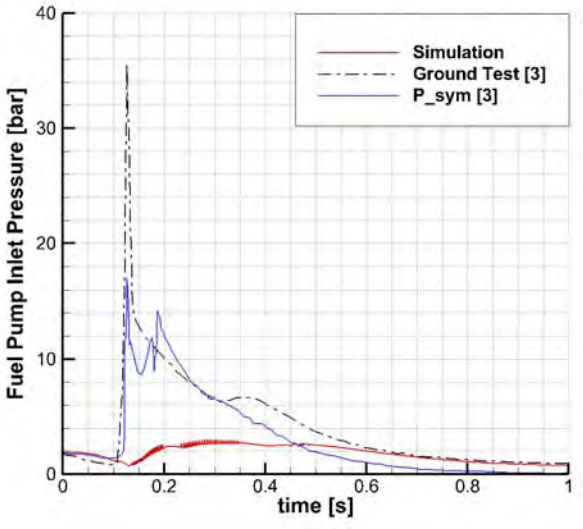

(c) Fuel Pump Inlet Pressure

Figure 15: Shut-down results - part 3

6 Conclusion

The major goals set for this work were to create a transient model for liquid rocket engines, develop a procedure able to simulate and predict the transient phases for future rocket engines, and to validate the model with an existing liquid rocket engine, the RL-10A-3-3A. These goals have been accomplished.

The RL10 shut-down model has captured many interesting effects that occur during shut-down.

In Figure 13 (a) for example, the chamber pressure tail-off is well simulated showing a clear difference between the NASA model, where an elbow-like profile is present, and our model where the pressure profile follows the measured data. In Figure 14 (c) the oxygen mass flow presents a similar profile of the test measure. The discrepancies between the two results can be also ascribed to the uncertainties on the closing profile of the OINV valve.

From inspection of the plots, it appears that there are still unresolved differences between the predicted and measured engine deceleration rates.

The discrepancies can be tracked down to two main causes: first, the time scales of the shut-down processes are much smaller than the one from the start-up transient, and second the complex phenomena such as cavitation and blade to fluid interaction that are not taken into account into the present model.

Comparison of the transient behaviour of the engine during ground test and model predictions is in general very satisfactory. Although some uncertainties affect the transient simulation the model correctly reproduces the main phenomena occurring during transients, such as ignition, heat transfer, turbopump operation phase change, valve manoeuvring and pressure drops, as well as the thermodynamic behaviour of the fluids.

Acknowledgements

The present study has been carried out in cooperation with ESA-ESTEC in the framework of the Networking and Partnering Initiative (NPI) Programme.

The authors would also like to acknowledge Mr. Thomas M. Tomsik from NASA who kindly supported us with information regarding the combustion chamber and cooling jacket geometry profile.

References

[1] M. Binder. An RL10A-3-3A Rocket Engine Model Using the Rocket Engine Transient Simulator (ROCETS) Software. Contractor Report NASA CR-190786, NASA, July 1993.

[2] M. Binder. A Transient Model of the RL10A-3-3A Rocket Engine. Contractor Report NASA CR-195478, NASA, July 1995.

[3] M. Binder, T. Tomsik, and J.P. Veres. RL10A-3-3A Rocket Engine Modeling Project. Technical Memorandum NASA TM-107318, NASA, 1997.

[4] H. Chaudhry. *Applied Hydraulic Transients - 2nd Edition*. Van Nostrand Reinhold Company, New York, 1987.

[5] F. Di Matteo, M. De Rosa, and M. Onofri. Semi-Empirical Heat Transfer Correlations in Combustion Chambers for Transient System Modelling. In 3AF, editor, *Space Propulsion Conference 2010*, San Sebastian, Spain, May 2010.

[6] F. Di Matteo, M. De Rosa, and M. Onofri. Start-Up Transient Simulation of a Liquid Rocket Engine. In *AIAA/SAE/ASME/ASEE 47th Joint Propulsion Conference and Exhibit*, number AIAA-2011-6032, 2011.

[7] Empresarios Agrupados. ESPSS user manual. 2.0 edition, 2010.

[8] Sanford Gordon and Bonnie J. McBride. Computer program for calculation of complex chemical equilibrium compositions and applications. Technical Report RP-1311, NASA, 1994.

[9] M. S. Haberbusch, C. T. Nguyen, and A. F. Skaff. Modeling RL10 Thrust Increase with Densified LH2 and LOX Propellants. In AIAA, editor, *39th AIAA/ASME/SAE/ASEE Joint Propulsion Conference and Exhibit*, number AIAA 2003-4485, July 2003.

[10] M. S. Haberbusch, A. F. Skaff, and C. T. Nguyen. Modeling the RL-10 with Densified Liquid Hydrogen and Oxygen Propellants. In AIAA, editor, *38th AIAA/ASME/SAE/ASEE Joint Propulsion Conference & Exhibit*, number AIAA 2002-3597, July 2002.

[11] P.J. Linstrom and W.G. Mallard. *NIST Chemistry WebBook, NIST Standard Reference Database Number 69*. National Institute of Standards and Technology, Gaithersburg MD, 20899, 2011. http://webbook.nist.gov, (retrieved July 14, 2011).

[12] Pratt&Whitney. Design Report For RL10A-3-3 Rocket Engine. Contractor Report CR-80920, NASA, 1966.

[13] A. J. Stepanoff. *Centrifugal and Axial Flow Pumps, 2nd edition*. J. Wiley and Sons, 1957.

[14] T. M. Tomsik. A Hydrogen-Oxygen Rocket Engine Coolant Passage Design Program (RECOP) for Fluid-cooled Thrust Chambers and Nozzles. Technical Note NASA-N95-70893, NASA, 1994.